ARTICLE NO. 80-0098R

Time-Dependent Difference Theory for Noise Propagation in a Two-Dimensional Duct

Kenneth J. Baumeister*
NASA Lewis Research Center, Cleveland, Ohio

A time-dependent numerical formulation is derived for sound propagation in a two-dimensional, straight, soft-walled duct in the absence of mean flow. The time-dependent governing acoustic-difference equations and boundary conditions are developed along with the maximum stable time increment. Example calculations are presented for sound attenuation in hard- and soft-wall ducts. The time-dependent analysis has been found to be superior to the conventional steady numerical analysis because of much shorter solution times and the elimination of matrix storage requirements.

Nomenclature

a_m, b_m, c_m, d_m
e_m, f_m, g_m = cell coefficients
c_0^* = ambient speed of sound, m/s
f^* = frequency, Hz
H^* = height of duct, m
I = number of axial grid points
i = $\sqrt{-1}$
J = number of transverse grid points
L^* = length of duct, m
n = transverse mode number
P = time-dependent acoustic pressure, $P^*/\rho_0^* c_0^{*2}$
p = spatially dependent acoustic pressure
p_s = spatially dependent solution of Helmholtz equation
T^* = period, $1/f^*$, s
t = dimensionless time, t^*/T^*
Δt = time step
u = axial acoustic velocity, u^*/c_0^*
v = transverse acoustic velocity, v^*/c_0^*
x = axial coordinate, x^*/H^*
Δx = axial grid spacing
y = dimensionless transverse coordinate, y^*/H^*
Δy = transverse grid spacing
Z^* = impedance, kg/m^2·s
α = stability factor
ζ = specific acoustic impedance
η = dimensionless frequency, $H^* f^*/c_0^*$
θ = dimensionless resistance
ρ_0^* = ambient air density, kg/m^3
χ = dimensionless reactance
ω = angular frequency

Subscripts

c = calculational time
e = exit condition
i = axial index (Fig. 1)
j = transverse index (Fig. 1)
m = cell index
0 = ambient condition

Superscripts

$*$ = dimensional quantity
k = time step
(1) = real part
(2) = imaginary part

Presented as Paper 80-0098 at the AIAA 18th Aerospace Sciences Meeting, Pasadena, Calif., Jan. 14-16, 1980; submitted Jan. 16, 1980; revision received April 28, 1980. This paper is declared a work of the U.S. Government and therefore is in the public domain.
Index categories: Aeroacoustics; Aerodynamics.
*Aerospace Engineer.

Introduction

BOTH finite-difference and finite-element numerical techniques[1-27] have been developed to study sound propagation with axial variations in Mach number, wall impedance, and duct geometry as might be encountered in a typical turbojet engine. Generally, the numerical solutions have been limited to low-frequency sound and short ducts, because many grid points or elements were required to resolve the axial wavelength of the sound. As shown in Ref. 1 [Eq. (77)] for plane wave propagation, the number of grid points or elements is proportional to the sound frequency and duct length, and inversely proportional to one minus the Mach number (Ref. 2, Fig. 6). This later dependence severely limits the application of numerical techniques for high Mach number inlets.

Customarily, the pressure and acoustic velocities are assumed to be simple harmonic functions of time; thus, the governing linearized gasdynamic equations (Ref. 28, p. 5) become independent of time. The matrices associated with the numerical solution to the time-independent equations must be solved exactly using such methods as Gauss elimination. Iteration techniques are unstable. As a result, large arrays of matrix elements must be stored which tax the storage capacity of even the largest computer. Sparse-matrix techniques[8,14,24] have been employed to reduce computer storage and run times as much as possible.

In unpublished work at Lewis using Ref. 29 as well as the work of Quinn (Ref. 23, p. 3) the matrix has been modified to allow iteration techniques; unfortunately, the convergence is too slow to be of any practical value. Other approaches, such as in Ref. 30, might still offer iterative possibilities.

Some special techniques have been developed to overcome the above-mentioned difficulties. As shown in Refs. 3 and 10, the wave envelope numerical technique can reduce the required number of grid points by an order of magnitude. In Ref. 20, this technique was used to optimize multielement liners of long lengths at high frequencies. At the present time, this technique has been applied only to the simple cases of no flow and plug flow. A numerical spatial marching technique was also developed in Refs. 15 and 18. Compared to the standard finite-difference or finite-element boundary value approaches, the numerical marching technique is orders of magnitude shorter in computational time and required

computer storage. The marching technique is limited to high frequencies and when reflections are small.

As an alternative to the previously developed steady-state theories, a time-dependent numerical technique is developed herein for noise propagation in a two-dimensional, soft-wall duct in the absence of mean flow. Advantageously, matrix storage requirements are significantly reduced in the time-dependent analysis. The analysis begins with a noise source radiating into an initially quiescent duct. This explicit method calculates stepwise in real time to obtain the transient as well as the "steady"-state solution of the acoustic field. The total time required for the analysis to calculate the "steady"-state acoustic field will determine the usefulness of the time-dependent technique.

Time-dependent numerical techniques have been applied extensively to both one-dimensional sound propagation (Ref. 31, p. 258), two-dimensional vibration problems (Ref. 32, p. 452), and the more general problem of compressible fluid flow.[33] References 31, 34, and 35 discuss in detail the stability of numerical solutions to the wave equation. Herein, these techniques will be extended to include soft-wall impedance boundary conditions which would be encountered in inlets and exhaust ducts of turbofan engines.

In the present paper, the governing acoustic-difference equation and the appropriate boundary conditions associated with time-dependent propagation are presented. Next, the von Neumann method is used to develop the relationship between sound frequency and grid spacing to determine the maximum stable time increment. Immediately following the mathematical development, numerical solutions are presented for one- and two-dimensional hard- and soft-wall ducts. The results are compared with the corresponding steady analytical results. Finally, the time required to perform both the time-dependent and steady analyses are compared for increasing number of grid points.

Governing Equations and Boundary Conditions

The propagation of sound in a two-dimensional rectangular duct, as shown in Fig. 1, is described by the linearized continuity and momentum equations and the appropriate impedance boundary conditions.

Continuity and Momentum

The linearized equations for mass and momentum conservation can be written (Ref. 28, p. 5) for a Cartesian coordinate system in the following dimensionless form:

$$\frac{\partial P}{\partial t} = -\frac{1}{\eta}\frac{\partial u}{\partial x} - \frac{1}{\eta}\frac{\partial v}{\partial y} \tag{1}$$

$$\frac{\partial u}{\partial t} = -\frac{1}{\eta}\frac{\partial P}{\partial x} \tag{2}$$

$$\frac{\partial v}{\partial t} = -\frac{1}{\eta}\frac{\partial P}{\partial y} \tag{3}$$

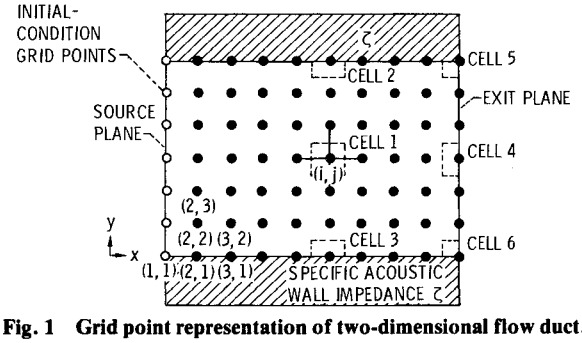

Fig. 1 Grid point representation of two-dimensional flow duct.

These and other symbols are defined in the nomenclature. The dimensionless frequency η is defined as

$$\eta = \left(\frac{H^*}{2\pi}\right)\frac{\omega^*}{c_0^*} = \frac{H^* f^*}{c_0^*} \tag{4}$$

The asterisks denote dimensional quantities.

The foregoing dimensionless equations apply to the scaled Cartesian coordinate system in which the height ranges between 0 and 1 and the dimensionless length ranges between 0 and L^*/H^*.

Wave Equation

Equations (1-3) now are combined to yield the dimensionless wave equation

$$\eta^2\frac{\partial^2 P}{\partial t^2} = \frac{\partial^2 P}{\partial x^2} + \frac{\partial^2 P}{\partial y^2} \tag{5}$$

Equation (5) in difference form will be solved to determine the pressure in the duct.

Wall Boundary Condition

The boundary condition at the surface of a sound absorbent soft-wall duct can be expressed in terms of a specific acoustic impedance defined as

$$\zeta = Z^*/\rho^* c_0^* = P/v \tag{6}$$

Substituting Eq. (6) into Eq. (3) yields

$$\frac{\partial P}{\partial y} = -\frac{\eta}{\zeta}\frac{\partial P}{\partial t} + \frac{\eta P}{\zeta^2}\frac{\partial \zeta}{\partial t} \tag{7}$$

In the example problems to be considered, the impedance will be assumed constant with time. Therefore, Eq. (7) reduces to

$$\frac{\partial P}{\partial y} = -\frac{\eta}{\zeta}\frac{\partial P}{\partial t} \tag{8}$$

At the lower wall, the sign on ζ is changed to account for the vector nature of v. As an alternate to this sign change, the velocity term in Eq. (6) can be dotted with the outward unit normal [Ref. 6, Eq. (9)]. It is also convenient to express the specific acoustic impedance in terms of resistance θ and reactance χ as

$$\zeta = \theta + i\chi \tag{9}$$

Entrance Condition

The boundary condition at the source plane $P(0,y,t)$ can be of any general form with both transverse variations in pressure and multiple frequency content. However, the numerical technique will be compared later to previous solutions in which the pressure and acoustic velocities were assumed to be plane waves at the entrance and to vary as $e^{i\omega^* t^*}$ or in dimensionless form as $e^{i2\pi t}$. Therefore, the source boundary condition used here is

$$P(0,y,t) = e^{i2\pi t} \qquad t > 0 \tag{10}$$

Exit Impedance

In a manner similar to the wall impedance, the axial impedance at the duct exit can be defined as

$$\zeta_e = \frac{P(L^*/H^*,y,t)}{u(L^*/H^*,y,t)} \tag{11}$$

For the plane wave propagation to be considered herein, ζ_e is taken as 1, which is exact for plane wave propagation in an

infinite hard-wall duct. Also choosing ζ_e to be 1 has lead to close agreement between numerical and analytical results for plane wave propagation into a soft-wall duct.[1,3] More general values for the exit impedance can be found in Refs. 7, 15 [Eq. (B4)], 16, or 18 (Fig. 7).

Initial Condition

For times equal to or less than zero, the duct is assumed quiescent, that is, the acoustic pressure and velocities are taken to be zero. For times greater than zero, the application of the noise source [Eq. (10)] will drive the pressures in the duct.

Complex Notation

Because of the introduction of complex notation for the noise source and wall impedances, all the dependent variables are complex. The superscript (1) will represent the real term while (2) will represent the imaginary term:

$$P=P^{(1)}+iP^{(2)} \tag{12}$$

A similar notation applies to the acoustic velocities.

Difference Equations

Instead of a continuous solution for pressure in space and time, the finite-difference approximations will determine the pressure at isolated grid points in space as shown in Fig. 1 and at discrete time steps Δt. Starting from the known initial conditions at $t=0$ and the boundary conditions, the finite-difference algorithm will march out the solution to later times.

Central Region (Cell 1)

Away from the duct boundaries, in cell 1 of Fig. 1, the second derivatives in the wave equation [Eq. (5)] can be represented by the usual central differences in time and space (Ref. 34, p. 99)

$$\eta^2\left[\left(P_{i,j}^{k+1}-2P_{i,j}^{k}+P_{i,j}^{k-1}\right)/\Delta t^2\right]=\left[\left(P_{i+1,j}^{k}-2P_{i,j}^{k}+P_{i-1,j}^{k}\right)/\Delta x^2\right]+\left[\left(P_{i,j+1}^{k}-2P_{i,j}^{k}+P_{i,j-1}^{k}\right)/\Delta y^2\right] \tag{13}$$

where i and j denote the space indices, k the time index, and Δx, Δy, and Δt are the space and time mesh spacing, respectively. All spacings are assumed constant. The time is defined as

$$t^{k+1}=t^k+\Delta t=(k+1)\Delta t \tag{14}$$

Solving Eq. (13) for the pressure $P_{i,j}^{k+1}$ yields

$$P_{i,j}^{k+1}=2P_{i,j}^{k}-P_{i,j}^{k-1}+\left\{\alpha\Big/\left[1+\left(\frac{\Delta y}{\Delta x}\right)^2\right]\right\}\left\{\left(\frac{\Delta y}{\Delta x}\right)^2 P_{i-1,j}^{k}+P_{i,j-1}^{k}-2\left[1+\left(\frac{\Delta y}{\Delta x}\right)^2\right]P_{i,j}^{k}+P_{i,j+1}^{k}+\left(\frac{\Delta y}{\Delta x}\right)^2 P_{i+1,j}^{k}\right\} \tag{15}$$

where α is defined as

$$\alpha=\frac{\Delta t^2}{\eta^2\Delta y^2}\left[1+\left(\frac{\Delta y}{\Delta x}\right)^2\right] \tag{16}$$

Equation (15) is an algorithm which permits marching-out solutions from known values of pressures at times associated with k and $k-1$. The procedure is explicit since all the past values of P^k are known as the new values of $k+1$ are computed. For the special case at $t=0$, the values of the pressure associated with the $k-1$ value are zero from the assumed initial condition. The parameter α was introduced into Eq. (15) because it will play an important role in determining the stability (error growth) of Eq. (15) in this explicit iteration scheme.

Boundary Condition (Cells 2-6)

The expression for the difference equations at the wall boundary are complicated by the impedance condition and the change in geometry of cells 2-6 in Fig. 1. The governing difference equations can be developed by an integration process in which the wave equation [Eq. (5)] is integrated over the area of the cells and time:

$$\int_{t-\Delta t/2}^{t+\Delta t/2}\iint_{\substack{\text{cell}\\ \text{area}}}\left(\eta^2\frac{\partial^2 P}{\partial t^2}-\frac{\partial^2 P}{\partial x^2}-\frac{\partial^2 P}{\partial y^2}\right)\mathrm{d}x\mathrm{d}y\mathrm{d}t=0 \tag{17}$$

The spatial integration over the cell area is fully documented in Ref. 10, Appendix D. In Eq. (17) of this paper, the spatial integration method of Ref. 10 has been extended to include time. An illustration of the application of Eq. (17) to cell 2 is given in the Appendix of this paper.

The finite-difference approximation for the various cells shown in Fig. 1 are expressed in terms of the cell coefficients a_m through g_m:

$$P_{i,j}^{k+1}=\frac{\alpha}{\left[1+(\Delta y/\Delta x)^2-\alpha f_m\right]}\left(a_m P_{i-1,j}^{k}+b_m P_{i,j-1}^{k}+\left\{c_m+\frac{2\left[1+(\Delta y/\Delta x)^2\right]}{\alpha}\right\}P_{i,j}^{k}+d_m P_{i,j+1}^{k}+e_m P_{i+1,j}^{k}\right)-\frac{\left[1+(\Delta y/\Delta x)^2-\alpha g_m\right]}{\left[1+(\Delta y/\Delta x)^2-\alpha f_m\right]}P_{i,j}^{k-1} \tag{18}$$

The subscript m denotes the cell number. These coefficients are listed in Table 1.

Spatial Mesh Size

The mesh spacing Δx and Δy must be restricted to small values to reduce the truncation error. To resolve the oscillatory nature of the pressure the required number of grid points in the axial direction suggested in Ref. 1 was

$$I\geq 12\eta(L^*/H^*) \tag{19}$$

No requirement for the size of transverse spacing Δy was given in Ref. 1 other than the number of transverse grid points be increased until convergence is achieved.

In the rectangular duct shown in Fig. 1, propagating transverse acoustic pressure modes ($\cos n\pi y$) can exist in the duct [Ref. 15, Eq. (B2)] when

$$n\leq 2\eta \tag{20}$$

To resolve all the propagating modes, the number of grid points in the transverse direction J suggested here is

$$J\geq 12\eta \tag{21}$$

Equation (19) in conjunction with Eq. (21) would lead to equal axial and transverse mesh spacing which generally minimizes the truncation error (Ref. 33, p. 288).

Stability

In the explicit time marching approach used here, round-off errors can grow in an unbounded fashion and destroy the solution if the time increment Δt is taken too large. The von Neumann method is often used to study the stability of the difference approximations to the wave equation. Application of the von Neumann method (Ref. 34, p. 104) to Eq. (13) requires that α in Eq. (16) be less than 1, which limits the time

Table 1 Coefficients in difference equations

Cell index, m	Difference elements[a] a_m	b_m	c_m	d_m	e_m	f_m	g_m
1	$\left(\frac{\Delta y}{\Delta x}\right)^2$	1	$-2\left[1+\left(\frac{\Delta y}{\Delta x}\right)^2\right]$	1	$\left(\frac{\Delta y}{\Delta x}\right)^2$	0	0
2	a_1	2	c_1	0	e_1	$-\frac{\eta}{\zeta}\frac{\Delta y}{\Delta t}$	$\frac{\eta}{\zeta}\frac{\Delta y}{\Delta t}$
3	a_1	0	c_1	2	e_1	$-\frac{\eta}{\zeta}\frac{\Delta y}{\Delta t}$	$\frac{\eta}{\zeta}\frac{\Delta y}{\Delta t}$
4	$2a_1$	1	c_1	1	0	$-\frac{\eta\Delta y^2}{\zeta_e\Delta t\Delta x}$	$\frac{\eta\Delta y^2}{\zeta_e\Delta t\Delta x}$
5	$2a_1$	2	c_1	0	0	f_2+f_4	g_2+g_4
6	$2a_1$	0	c_1	2	0	f_3+f_4	g_3+g_4

[a] $\Psi_m = a_m P^k_{i-1,j} + b_m P^k_{i,j-1} + c_m P^k_{i,j} + d_m P^k_{i,j+1} + e_m P^k_{i+1,j} + f_m P^{k+1}_{i,j} + g_m P^{k-1}_{i,j}$.

increment

$$\Delta t \leqq \eta \Delta y \Big/ \sqrt{1+\left(\frac{\Delta y}{\Delta x}\right)^2} \tag{22}$$

The derivation in Ref. 34 was for only one space dimension; however, the extension of the von Neumann method to two space dimensions is relatively easy. When the time step satisfies Eq. (22), a condition of marginal stability exists (Ref. 34, p. 106), which guarantees that a propagating acoustic mode can travel undiminished in a hard-wall duct (see discussion, Ref. 18, p. 302).

Steady-State Pressures

In the sample problems to be presented in the next section, the time-dependent results will be compared to the results of the steady harmonic solutions of Ref. 10. The purpose of the section is to show the rationale for constructing a steady-state solution from the time-dependent results.

Steady Harmonic Solution

The steady harmonic pressure $p_s(x,y)$ is defined as a solution to Eq. (5) when the pressure is assumed to be a simple harmonic function of time:

$$P(x,y,t) = p_s(x,y)e^{i2\pi t} \tag{23}$$

Substituting Eq. (23) into Eq. (5), the wave equation takes the form of the classic Helmholtz equation

$$\frac{\partial^2 p_s}{\partial x^2} + \frac{\partial^2 p_s}{\partial y^2} + (2\pi\eta)^2 p_s = 0 \tag{24}$$

In this case, where the source is a simple harmonic function of time, p_s represents the Fourier transform of $P(x,y,t)$ (Ref. 28, p. 11). The boundary conditions can also be modified by Eq. (23) as shown in Ref. 10.

For a semi-infinite duct (or an equivalent finite duct with $\rho^* c_0^*$ exit impedance) with plane wave propagation and hard walls, the solution for p_s is

$$p_s = e^{-i2\pi\eta x} \tag{25}$$

In the next section, a transient solution to this problem will be compared to Eq. (25).

Transient Solution

Recall, at the start of the numerical calculation, the acoustic pressures and velocities were assumed zero throughout the duct and a pressure source begins a harmonic oscillation at $x=0$ for $t>0$. For the special case of plane wave propagation in a hard-wall, semi-infinite duct, the analytical solution to the wave equation [Eq. (5)] is (Ref. 36, p. 305)

$$P(x,t) = \begin{cases} 0 & 0<t<\eta x \quad (26) \\ e^{-i2\pi\eta x}e^{i2\pi t} & t>\eta x \quad (27) \end{cases}$$

The pressure $p(x,y)$ is now defined by dividing the instantaneous pressure $P(x,y,t)$ by $e^{i2\pi t}$ to obtain

$$p(x,y) = P(x,y,t)/e^{i2\pi t} \tag{28}$$

Using this definition, Eqs. (26) and (27) become

$$p(x) = \begin{cases} 0 & 0<t<\eta x \quad (29) \\ e^{-i2\pi\eta x} & t>\eta x \quad (30) \end{cases}$$

Consequently, the transient solution [Eq. (30)] for the steady harmonic pressure equals the Fourier transform solution [Eq. (25)] when

$$t > \eta x \tag{31}$$

In terms of real variables, Eq. (31) can be written as

$$t^* > x^*/c_0^* \tag{32}$$

The transient time t^* represents the time for the wave to travel down to the end of the duct, $x^*=L^*$. Therefore, for the special case of one-dimensional plane wave propagation, the initial transient will pass when Eq. (31) holds.

Since it may be desirable to integrate the wave with time to obtain a rms (root mean square) pressure, the transient calculations will be continued into the steady domain for one period of oscillation before the Fourier pressure p is calculated. Therefore, in this paper,

$$t_c = \eta(L^*/H^*) + 1 \tag{33}$$

and

$$p(x,y) = P(x,y,t)/e^{i2\pi t_c} \tag{34}$$

For more complicated problems, such as with higher order acoustic pressure modes or where reflections are important, t_c should be increased in successive steps to check for convergence.

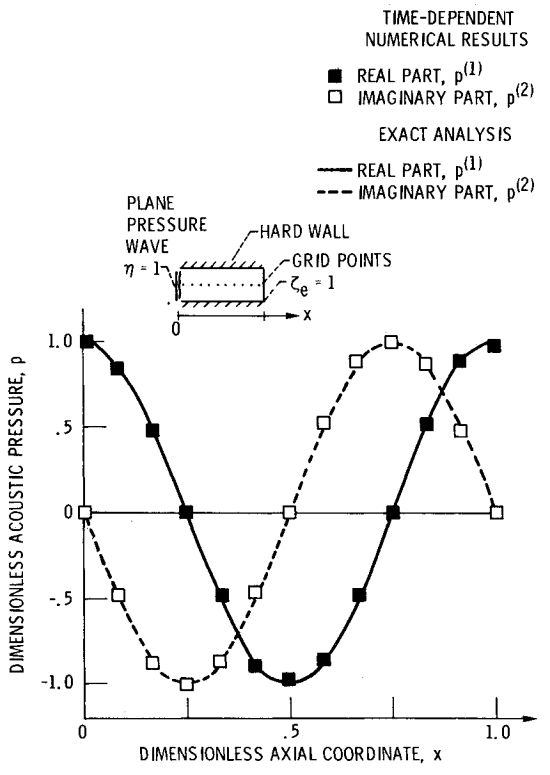

Fig. 2 Analytical and numerical pressure profiles for one-dimensional plane wave sound propagation in hard-wall duct for $\eta = 1$ and $L^*/H^* = 1$.

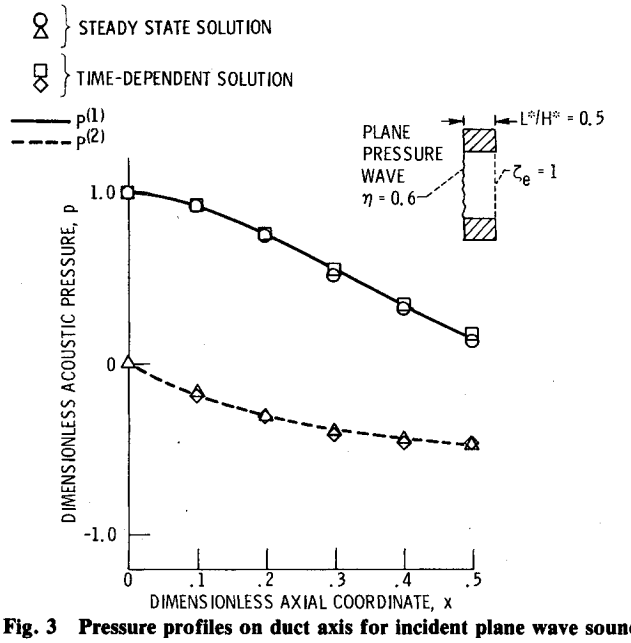

Fig. 3 Pressure profiles on duct axis for incident plane wave sound propagation in soft-wall duct ($\eta = 0.6$, $L^*/H^* = 0.5$, $\zeta_w = 0.16 - i0.34$).

Sample Calculations

In two sample problems to follow, the time-dependent results will be compared to the results of the steady harmonic solutions of Ref. 10.

Hard-Wall Duct

Numerical and analytical values of the pressure $p(x,y)$ are computed for the case of a hard-wall duct for plane wave propagation with $\zeta_e = 1$ exit impedance (equivalent to semi-infinite duct). The calculation was made with a length to height ratio (L^*/H^*) of 1 and a dimensionless frequency η of 1. The analytical and numerical values of the acoustic pressure profiles along the duct are shown in Fig. 2. As seen in Fig. 2, agreement between analytical and the numerical theory is good.

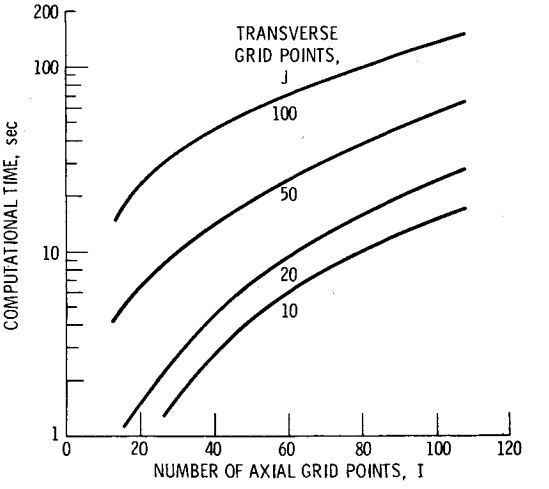

Fig. 4 Effect of increasing number of grid points on calculational time of transient solution for plane wave propagation in hard-wall duct ($\eta = 1$, $L^*/H^* = 1$).

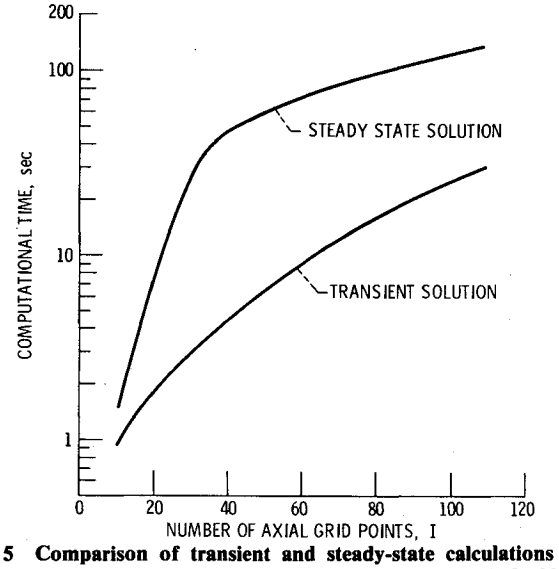

Fig. 5 Comparison of transient and steady-state calculations for plane wave propagation in hard-wall duct ($\eta = 1$, $L^*/H^* = 1$, $J = 20$).

Soft-Wall Duct

As another example of the time-dependent analysis, the pressure distributions are computed for the case of plane wave propagation with a $\zeta_e = 1$ exit impedance and a wall with impedance values of $0.16 - i0.34$. The calculation was made with a length-to-height ratio of 0.5 and a dimensionless frequency of 0.6. The results of the time-dependent analysis along with the results of the solution of the equivalent steady-state Helmholtz equation are displayed in Fig. 3. The numerical results for the steady spatial solution $p_s(x,y)$ are tabulated in Appendix F of Ref. 10. As seen in Fig. 3, again the steady and time-dependent analyses are in good agreement.

Grid Point Variations

Figure 4 shows the effect of increasing the number of grid points on the computational time of the time-dependent approach for the hard-wall duct associated with Fig. 2. Roughly, as seen in Fig. 4, the computational time is

proportional to the 1.5 power of the total grid points, as would be predicted from Eq. (22) for equal Δx and Δy. Theoretically, the total computational time is proportional to the number of grid points and the reciprocal of the time increment.

Figure 5 shows a comparison of the computational times for the steady and time-dependent problems associated with the hard-wall duct shown in Fig. 2. As seen in this figure, the time-dependent analysis is considerably faster than the steady analysis. The value of J (grid points in y direction) was restricted to 20 because of practical limitations on the size of the matrix which could be effectively handled in the steady analysis. When J was increased to 50 with 50 axial grid points, the steady analysis required 5500 s as compared to less than 20 s for the time-dependent analysis. This large increase in the steady-state solution time results because of the manner in which the general matrix was partitioned (Ref. 10, p. 14). An out-of-core banded solver was used with a moderate amount of in-core storage but much more input/output time.

Finally these calculations were performed on the Univac 1100 computer. Faster computers can be expected to reduce these calculational times significantly.

Conclusions

The numerical time-dependent method of analysis represents a significant advance over previous steady numerical theories. By eliminating large matrix storage requirements, numerical calculations of high sound frequencies are now possible. Also, because matrix manipulation is not required, the time-dependent approach is simpler to program and debug. Although flow has not been considered herein, the extension to the more general flow situation apears to be straightforward.

Appendix: Finite-Difference Equations and Coefficients

The derivation of the difference equation for the various cell starts with Eq. (17), which is rewritten here as

$$\int_{t-\Delta t/2}^{t+\Delta t/2}\int_{-}^{+}\int_{-}^{+}\left(\eta^2\frac{\partial^2 P}{\partial t^2}-\frac{\partial^2 P}{\partial x^2}-\frac{\partial^2 P}{\partial y^2}\right)dx\,dy\,dt=0 \tag{A1}$$

where the plus sign (+) in the upper limit of integration means to evaluate the parameters along either the upper or right-hand boundary of the integration cell shown in Fig. 1 by the dashed lines, while the negative sign (−) applies to either the lower or left-hand boundary of the integration cell, depending upon whether x or y is considered. The (+) and (−) notation was used since the spatial integration limits will vary from cell to cell. For cell 2 for example, in the x integral, (+) is represented by $x+\Delta x/2$ and (−) by $x-\Delta x/2$, while in the y integral, (+) is represented by 1 and (−) by $1-\Delta y/2$.

The pressure P can be assumed constant over the cell area and likewise the second derivative in time can also be assumed constant over the entire cell area. Therefore, moving the spatial derivatives to the right side of Eq. (A1) gives

$$\eta^2\int_{t-\Delta t/2}^{t+\Delta t/2}\frac{\partial^2 P_{i,j}}{\partial t^2}dt\left(\int_{-}^{+}\int_{-}^{+}dx\,dy\right)=\int_{t-\Delta t/2}^{t+\Delta t/2}\times\int_{-}^{+}\int_{-}^{+}\left(\frac{\partial^2 P}{\partial x^2}+\frac{\partial^2 P}{\partial y^2}\right)dx\,dy\,dt \tag{A2}$$

but

$$\int_{t-\Delta t/2}^{t+\Delta t/2}\frac{\partial^2 P}{\partial t^2}dt=\frac{\partial P}{\partial t}\Big|_{t-\Delta t/2}^{t+\Delta t/2}=\left(\frac{P_{i,j}^{k+1}-P_{i,j}^{k}}{\Delta t}\right)-\left(\frac{P_{i,j}^{k}-P_{i,j}^{k-1}}{\Delta t}\right)=\frac{P_{i,j}^{k+1}-2P_{i,j}^{k}+P_{i,j}^{k-1}}{\Delta t} \tag{A3}$$

Therefore, Eq. (A2) can be written as

$$P_{i,j}^{k+1}=2P_{i,j}^{k}-P_{i,j}^{k-1}+\frac{\alpha}{[1+(\Delta y/\Delta x)^2]}\Psi_m \tag{A4}$$

where

$$\Psi_m=\frac{\Delta y^2}{\Delta t}\int_{t-\Delta t/2}^{t+\Delta t/2}\left[\int_{-}^{+}\left(\frac{\partial P}{\partial x}\Big|^{+}-\frac{\partial P}{\partial x}\Big|_{-}\right)dy+\int_{-}^{+}\left(\frac{\partial P}{\partial y}\Big|^{+}-\frac{\partial P}{\partial y}\Big|_{-}\right)dx\right]dt \tag{A5}$$

The parameter Ψ_m can now be evaluated for each cell (labeled m) in Fig. 1. The procedure for each cell is given in detail in Ref. 10, Appendix D. To illustrate how the time integration is coupled to the space integration, the derivation for cell 2 will now be presented.

For cell 2,

$$\int_{-}^{+}\int_{-}^{+}dy\,dx=\frac{\Delta y\Delta x}{2} \tag{A6}$$

$$\frac{\partial P}{\partial x}\Big|^{+}-\frac{\partial P}{\partial x}\Big|_{-}=\left(\frac{P_{i+1,j}^{k}-P_{i,j}^{k}}{\Delta x}\right)-\left(\frac{P_{i,j}^{k}-P_{i-1,j}^{k}}{\Delta x}\right)=\frac{P_{i+1,j}^{k}-2P_{i,j}^{k}+P_{i-1,j}^{k}}{\Delta x} \tag{A7}$$

$$\frac{\partial P}{\partial y}\Big|^{+}-\frac{\partial P}{\partial y}\Big|_{-}=-\frac{\eta}{\zeta}\frac{\partial P_{i,j}}{\partial t}-\left(\frac{P_{i,j}^{k}-P_{i,j-1}^{k}}{\Delta y}\right) \tag{A8}$$

The expression for $\partial P/\partial y\,|^{+}$ in Eq. (A8) is the wall boundary condition as given by Eq. (8). Substituting Eqs. (A6-A8) into Eq. (A5) yields

$$\Psi_2=\frac{2}{\Delta t}\frac{\Delta y}{\Delta x}\left[\left(\frac{P_{i+1,j}^{k}-2P_{i,j}^{k}+P_{i-1,j}^{k}}{\Delta x}\right)\int_{t-\Delta t/2}^{t+\Delta t/2}\times dt\int_{-}^{+}dy-\frac{\eta}{\zeta}\int_{t-\Delta t/2}^{t+\Delta t/2}\frac{\partial P_{i,j}}{\partial t}dt\int_{-}^{+}\times dx-(P_{i,j}^{k}-P_{i,j-1}^{k})\int_{t-\Delta t/2}^{t+\Delta t/2}dt\int_{-}^{+}dx\right] \tag{A9}$$

Equation (A9) can be further simplified by noting

$$\int_{-}^{+}dy=\frac{\Delta y}{2} \tag{A10}$$

$$\int_{-}^{+}dx=\Delta x \tag{A11}$$

$$\int_{t-\Delta t/2}^{t+\Delta t/2}dt=\Delta t \tag{A12}$$

$$\int_{t-\Delta t/2}^{t+\Delta t/2}\frac{\partial P}{\partial t}dt=P_{i,j}\Big|_{t-\Delta t/2}^{t+\Delta t/2}=\left(\frac{P_{i,j}^{k+1}+P_{i,j}^{k}}{2}\right)-\left(\frac{P_{i,j}^{k}+P_{i,j}^{k-1}}{2}\right)=\frac{P_{i,j}^{k+1}-P_{i,j}^{k-1}}{2} \tag{A13}$$

Substituting Eqs. (A10-A13) into Eq. (A9) yields

$$\Psi_2=\left(\frac{\Delta y}{\Delta x}\right)^2P_{i-1,j}^{k}+2P_{i,j-1}^{k}-2\left[1+\left(\frac{\Delta y}{\Delta x}\right)^2\right]P_{i,j}^{k}+\left(\frac{\Delta y}{\Delta x}\right)^2P_{i+1,j}^{k}-\frac{\eta}{\zeta}\frac{\Delta y}{\Delta t}P^{k+1}+\frac{\eta}{\zeta}\frac{\Delta y}{\Delta t}P_{i,j}^{k-1} \tag{A14}$$

which contain the coefficients that appear in Table 1 for cell 2. The coefficients for the other cells are found in a similar manner.

References

[1] Baumeister, K. J. and Bittner, E. C., "Numerical Simulation of Noise Propagation in Jet Engine Ducts," NASA TN D-7339, 1973.

[2] Baumeister, K. J. and Rice, E. J., "A Difference Theory for Noise Propagation in an Acoustically Lined Duct with Mean Flow," *Progress in Astronautics and Aeronautics—Aeroacoustics: Jet and Combustion Noise; Duct Acoustics*, Vol. 37, AIAA, New York, 1975, pp. 435-453.

[3] Baumeister, K. J., "Analysis of Sound Propagation in Ducts Using the Wave Envelope Concept," NASA TN D-7719, 1974.

[4] Quinn, D. W., "A Finite Difference Method for Computing Sound Propagation in Nonuniform Ducts," AIAA Paper 75-130, Jan. 1975.

[5] Baumeister, K. J., "Waves Envelope Analysis of Sound Propagation in Ducts with Variable Axial Empedance," *Progress in Astronautics and Aeronautics—Aeroacoustics: Duct Acoustics, Fan Noise and Control Rotor Noise*, edited by I. R. Schwartz, H. T. Nagamatsu, and W. Strahle, Vol. 44, AIAA, New York, 1976, pp. 451-474.

[6] Quinn, D. W., "Attenuation of Sound Associated with a Plane Wave in a Multisectional Duct," *Progress in Astronautics and Aeronautics—Aeroacoustics: Duct Acoustics, Fan Noise and Control Rotor Noise*, edited by I. R. Schwartz, H. T. Nagamatsu, and W. Strahle, Vol. 44, AIAA, New York, 1976, pp. 331-345.

[7] Sigman, R. K., Majjigi, R. K., and Zinn, B. T., "Determination of Turbofan Inlet Acoustics Using Finite Elements," *AIAA Journal*, Vol. 16, Nov. 1978, pp. 1139-1145.

[8] Abrahamson, A. L., "A Finite Element Algorithm for Sound Propagation in Axisymmetric Ducts Containing Compressible Mean Flow," NASA CR-145209, Wyle Laboratories, Inc., Hampton, Va., June 1977.

[9] Craggs, A., "A Finite Method for Modelling Dissipative Mufflers with a Locally Reactive Lining," *Journal of Sound and Vibration*, Vol. 54, Sept. 1977, pp. 285-296.

[10] Baumeister, K. J., "Finite-Difference Theory for Sound Propagation in a Lined Duct with Uniform Flow Using the Wave Envelope Concept," NASA TP-1001, 1977.

[11] Kagawa, Y., Yamabuchi, T., and Mori, A., "Finite Element Simulation of an Axisymmetric Acoustic Transmission System with a Sound Absorbing Wall," *Journal of Sound and Vibration*, Vol. 53, Aug. 1977, pp. 357-374.

[12] Eversman, W., Astley, R. J., and Thanh, V. P., "Transmission in Nonuniform Ducts—A Comparative Evaluation of Finite Element and Weighted Residuals Computational Schemes," AIAA Paper 77-1299, Oct. 1977.

[13] Watson, W. R., "A Finite Element Analysis of Sound Propagation in a Rectangular Duct of Finite Length with Peripherally Variable Liners," AIAA Paper 77-1300, Oct. 1977.

[14] Abrahamson, A. L., "A Finite Element Algorithm for Sound Propagation in Axisymmetric Ducts Containing Compressible Mean Flow," AIAA Paper 77-1301, Oct. 1977.

[15] Baumeister, K. J., "Numerical Spatial Marching Techniques for Estimating Duct Attenuation and Source Pressure Profiles," *Proceedings of 95th Meeting of Acoustical Society of America*, Providence, R.I., May 16-19, 1978 (also NASA TM-78857, 1978).

[16] Tag, I. A. and Lumsdaine, E., "An Efficient Finite Element Technique for Sound Propagation in Axisymmetric Hard Wall Ducts Carrying High Subsonic Mach Number Flows," AIAA Paper 78-1154, July 1978.

[17] Astley, R. J. and Eversman, W., "A Finite Element Method for Transmission in Non-Uniform Ducts without Flow: Comparison with the Method of Weighted Residuals," *Journal of Sound and Vibration*, Vol. 57, April 1978, pp. 367-388.

[18] Baumeister, K. J., "Numerical Spatial Marching Techniques in Duct Acoustics," *Journal of the Acoustical Society of America*, Vol. 65, Feb. 1979, pp. 297-306.

[19] Majjigi, R. K., "Application of Finite Element Techniques in Predicting the Acoustic Properties of Turbofan Inlets," Ph.D. Thesis, Georgia Institute of Technology, Atlanta, Ga., 1979.

[20] Baumeister, K. J., "Optimized Multisectioned Acoustic Liners," AIAA Paper 79-0182, Jan. 1979.

[21] Majjigi, R. K., Sigman, R. K., and Zinn, B. T., "Wave Propagation in Ducts Using the Finite Element Method," AIAA Paper 79-0659, March 1979.

[22] Astley, R. J. and Eversman, W., "The Application of Finite Element Techniques to Acoustic Transmission in Lined Ducts with Flow," AIAA Paper 79-0660, March 1979.

[23] Quinn, D. W., "A Finite Element Method for Computing Sound Propagation in Ducts Containing Flow," AIAA Paper 79-0661, March 1979.

[24] Abrahamson, A. L., "Acoustic Duct Liner Optimization Using Finite Elements," AIAA Paper 79-0662, March 1979.

[25] Tag, I., A. and Akin, J. E., "Finite Element Solution of Sound Propagation in a Variable Area Duct," AIAA Paper 79-0663, March 1979.

[26] Lester, H. C. and Parrott, T. L., "Application of Finite Element Method for Computing Grazing Incidence Wave Structure in an Impedance Tube: Comparison with Experiment," AIAA Paper 79-0664, March 1979.

[27] Baumeister, K. J. and Majjigi, R. K., "Applications of Velocity Potential Function to Acoustic Duct Propagation and Radiation from Inlets Using Finite-Element Theory," AIAA Paper 79-0680, March 1979.

[28] Goldstein, M. E., *Aeroacoustics*, McGraw-Hill Book Co., New York, 1976.

[29] Beaubien, M. J. and Wesler, A., "Iterative, Finite Difference Solution of Interior Eigenvalues and Eigenfunctions of Laplace's Operator," *Computer Journal*, Vol. 14, Aug. 1971, pp. 263-269.

[30] Browne, B. T. and Lawrenson, P. J., "Numerical Solution of an Elliptic Boundary-Value Problem in the Complex Variable," *Institute of Mathematics and its Applications Journal*, Vol. 17, 1976, pp. 311-327.

[31] Richtmyer, R. D. and Morton, K. W., *Difference Methods for Initial-Value Problems*, 2nd Ed., Interscience, New York, 1967.

[32] Gerald, C. F., *Applied Numerical Analysis*, 2nd Ed., Addison-Wesley, Reading, Mass., 1978.

[33] Roache, P. J., *Computational Fluid Dynamics*, Hermosa, Albuquerque, N. Mex., 1972.

[34] Clark, M. and Hansen, K. F., *Numerical Methods of Reactor Analysis*, Academic Press, New York, 1964.

[35] Hildebrand, F. B., *Methods of Applied Mathematics*, Prentice-Hall, Englewood Cliffs, N.J.

[36] Budak, B. M., Samarskii, A. A., and Tikhonov, A. N., *A Collection of Problems on Mathematical Physics*, Pergamon Press, Oxford, England, 1964.